Journal of the Indian Institute of Science
A Multidisciplinary Reviews Journal
ISSN: 0970-4140 Coden-JIISAD

REVIEWS

Electrode Disorder, Electrochemical Processes and Governing Length Scales

Rama Kant, Shweta Dhillon and Jasmin Kaur*

Abstract | Surface of a solid electrode ubiquitously possesses morphological and energetic disorders, and therefore it greatly influences their thermodynamics, kinetics and transport properties. Also, the anomalies in an electrochemical response are governed by the synergistic effect of the morphological and phenomenological lengths. For theoretical understanding of disordered systems, it becomes mandatory to characterize these length scales, and their dependence on electrochemical and morphological characteristics. In this review, we mainly focus on two aspects: (1) statistical characterization of electrode surface using FE-SEM micrographs and electrochemical microscopic area, and (2) the physical significance of various length scales arising in theoretical models and electrode surface topography. Finally, a common scale is generated to show the synergistic effects of morphological and phenomenological length scales in disordered electrochemical system.

Keywords: *electrode topography, capacitance, transient response, phenomenological length scales, curvature, roughness*

1 Introduction

Surface disorder plays a significant role in determining the chemical, physical and electrochemical behavior of the interface (in many diffusion limited physico-chemical processes). Microstructured and nanostructured materials are currently of great interest for devices such as electrochemical sensors,[1–3] supercapacitors,[4] photovoltaics and fuel cells[5] because of their large surface area, novel size effects,[6] significantly enhanced kinetics, and so on. Solid planar electrodes are not smooth at all length scales as they exhibit complex surface morphology with varying degree of irregularity ranging from sub-nanometer to micrometer length scales.[7] The electrochemical properties of an electrode are affected by its composition, crystallographic features as well as morphology. This dependence causes emergence of anomalous electrochemical responses as they tend to deviate from the classical electrochemical behavior.[8]

In order to decipher the anomalies in the electrochemical responses, several theoretical frameworks have been presented. The fractional diffusion equation approach,[9,10] scaling approach,[11–13] equivalent circuit modeling[14–16] and perturbation approach[17,18] are some of the widely used approaches. The fractional diffusion approach can be used for diffusion towards an interface for porous media with fractal structure, and in diffusion of free carriers in multiple trapping. However, difficulty in obtaining the analytical solution of the problem and complicated mathematical operator structure limits its applicability. On the other hand, scaling approach can effectively interpret large quantity of data, but is unable to include a complete set of realistic fractal morphological parameters. Hence, it does not capture subtle aspects of experimental data and their crossover behaviors. The equivalent circuit approach requires rigorous presumptions of the fitting parameters, hence is often unable to capture the complexity and dynamics of the electrochemical systems. Our boundary shape and profile perturbation approach uses detailed geometry of the surface to model anomalous diffusion at the rough electrode surface. Kant and coworkers have established a series of relationships

Complex Systems Group, Department of Chemistry, University of Delhi, Delhi 110007, India.

*rkant@chemistry.du.ac.in

between the observables like current, admittance, absorbance and charge transients with the morphology of the electrodes via power spectrum of rough interface.[17–45] This method has advantages over the others since the solutions take the form of relatively simple explicit analytical expressions that can be evaluated much more easily.

Power spectrum: It performs a decomposition of the surface profile into its spatial wavelengths and expresses the roughness power per unit spatial frequency or wavenumber over the sampling length.

The following sections will attempt to describe various underlying concepts in electrode structure characterization and their correlation to the electrochemical processes with brief outlines of their length and time scales. Firstly, the study of electrode surface morphology through its stochastic modeling, finite fractal characterization and a method to extract various morphological quantities are discussed. In the next section, various phenomenological length scales are discussed based on the active electrochemical phenomena. Finally, the coupling of morphological and phenomenological length scales is established to unravel the causes of morphology induced anomalies in the electrochemical processes.

Correlation function: A function describing the statistical link between the random surface profiles distributed in spatial coordinates.

Coupling length: The characteristic phenomenological length scale emerging due to coupling of two or more phenomena in an electrochemical system.

2 Quantitative Electrode Roughness: Through FE-SEM Micrographs

Surface characterization is an imperative step for addressing relation between surface structures and surface electrochemical properties. Surface roughness (in sub-nm to 100 nm) can cause modification in work function and solvation of the electrode, therefore, transforms its thermodynamics and kinetics. Roughness also introduces random topographic confinements of diffusing particles near the surface and their influence persists till diffusion layer thickness exceeds the width of roughness. Hence, mass transport in multi-scale confined environment causes anomalous electrochemical responses. So, it becomes mandatory to characterize the surface structures over an electrode. Several techniques are available to analyze the morphology and roughness of the electrode surfaces. Quantitative surface characterization is done with the high resolution techniques such as FE-SEM (field emission scanning electron microscopy), AFM (atomic force microscopy) and STM (scanning tunneling microscopy). FE-SEM spatial resolution for surface morphology is comparable to AFM resolution, approximately 1 nm. Various length scales are involved with the surface morphology and can be obtained using FE-SEM, AFM etc. Roughness factor obtained from AFM are usually lower than the obtained from the electrochemical methods. In this section, we will focus on quantitative surface characterization from FE-SEM and electrochemically measured roughness factor.

The FE-SEM image of an electrode surface has random profile, which varies from sample to sample. Therefore, the electrode surface profile should be characterized through its statistical measures. The simplest measures of roughness are the roughness factor (R^* = microscopic area/projected area) and the mean square width of roughness (h^2). The more general characterization of the electrode surface roughness is the two-point height correlation function and even more useful quantity, its Fourier transform, the Power Spectrum (PS). For statistical characterization, the random electrode surface profile $\left(\zeta(\vec{r}_{\|})\right)$ can be looked upon as a homogeneous (stationary), isotropic, centered and Gaussian fields,[46]

$$\begin{aligned} \left\langle \zeta(\vec{r}_{\|}) \right\rangle &= 0 \\ \left\langle \zeta(\vec{r}_{\|})\zeta(\vec{r}'_{\|}) \right\rangle &= h^2 W(|\vec{r}_{\|} - \vec{r}'_{\|}|) \end{aligned} \qquad (1)$$

where $W(|\vec{r}_{\|} - \vec{r}'_{\|}|)$ is the correlation function of surface height fluctuations. Here, angular brackets denote an ensemble average over various possible surface configurations and $h^2 = \left\langle \zeta^2(\vec{r}_{\|}) \right\rangle$ denotes the mean square departure of the surface from flatness or the measure of width of the interface. The quantity that can be directly obtained from the FE-SEM micrographs or AFM profile measurement is the Fourier transform of the correlation function[19]

$$\begin{aligned} \left\langle \hat{\zeta}(\vec{K}_{\|}) \right\rangle &= 0 \\ \left\langle \hat{\zeta}(\vec{K}_{\|})\hat{\zeta}(\vec{K}'_{\|}) \right\rangle &= (2\pi)^2 \delta\left(\vec{K}_{\|} + \vec{K}'_{\|}\right) \left\langle \left| \hat{\zeta}(\vec{K}_{\|}) \right|^2 \right\rangle \end{aligned} \qquad (2)$$

where $\delta(\vec{K}_{\|})$ is the two-dimensional Dirac delta function in vector $\vec{K}_{\|}$. PS performs decomposition of the surface profile into its spatial wavelengths and allows the comparison of roughness measurements over different spatial frequency ranges.[47] The PS of roughness $(\langle |\hat{\zeta}(\vec{K}_{\|})|^2 \rangle)$ is the ensemble average of all the possible configurations. PS is defined as the ensemble average of the product of Fourier transform of surface profile $(\hat{\zeta}(\vec{K}_{\|}))$ and its complex conjugate $(\hat{\zeta}^*(\vec{K}_{\|}))$. For a slowly varying surface profile, it is compressed around the lower frequencies, whereas for a rapidly varying surface it is spread out in the higher frequency domain.

The FE-SEM images are directly related to the changes in height data, but they lack the exact information of height. Therefore, Figure 1 summarizes a recently developed method for surface characterization using FE-SEM micrographs and microscopic area from cyclic

voltammetry (CV).[48] In this method denoised images are used to extract the statistical information of roughness in the form of power spectral density (PSD). PSD extracted from denoised FE-SEM images is the scaled PSD as this is calculated from relative height information stored in FE-SEM images in morphological (secondary electron) mode. To convert scaled PSD data into quantitative PSD, roughness factor (R^*) information obtained from CV is used. The bridging relation between the roughness factor and the second moment of power spectrum or mean square gradient (MSG) of roughness (m_2) is given as[49,48]

$$R^* = 1 + \sqrt{\frac{\pi m_2}{2}} \exp\left(\frac{1}{2m_2}\right) \operatorname{erfc}\left(\frac{1}{\sqrt{2m_2}}\right) \quad (3)$$

Denoising: Process of removing artifacts in data ("salt and pepper noise") from a measured surface data, introduced by the device's mechanism or processing algorithm.

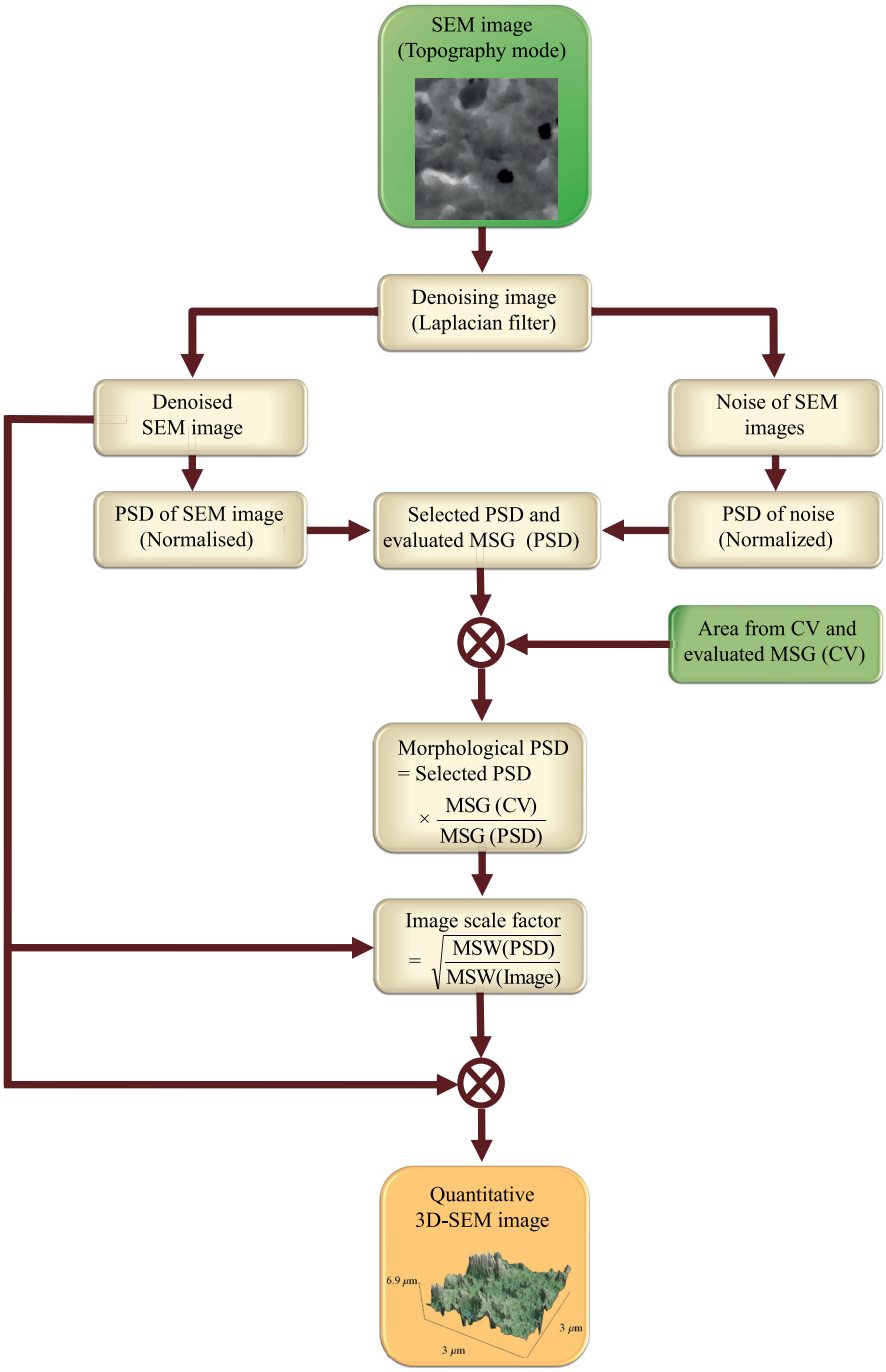

Figure 1: Flowchart of the algorithm employed for quantitative 3D reconstruction of electrode surface using microscopic area from cyclic voltammetry (CV) and morphology from semi-quantitative FE-SEM image.[48]

Equation 3 can be used to extract m_2 from the electrochemically obtained R^*. m_2 obtained from power spectrum is defined as,[48]

$$m_2 = \frac{1}{(2\pi)^2}\int d^2K_{\parallel}\, K_{\parallel}^2 \left\langle |\zeta(\vec{K}_{\parallel})|^2 \right\rangle \tag{4}$$

Mean square gradient obtained from scaled PSD and CV are compared to obtain a scale factor for the morphological PSD (Figure 1). The missing scale factor for normalized PSD is obtained as[48]

$$\text{PSD scale factor} = \frac{m_2(\text{CV})}{m_2(\text{SEM})} \tag{5}$$

Once the PSD scale factor for an electrode, is known, it is possible to know the quantitative PSD. Another useful quantity that is required to reconstruct the height profile from the FE-SEM micrographs is the mean square width (MSW), given as,[48]

$$m_0 = \frac{1}{(2\pi)^2}\int d^2K_{\parallel} \left\langle |\zeta(\vec{K}_{\parallel})|^2 \right\rangle \tag{6}$$

To reconstruct the 3D surface of an electrode from the FE-SEM micrograph, an image scale factor is required which is obtained as[48]

$$\text{Image scale factor} = \sqrt{\frac{m_0(\text{PSD})}{m_0(\text{image})}} \tag{7}$$

For further illustration, Figure 2 (a) shows the FE-SEM image of an electrochemically roughened platinum (roughening procedure given in Ref.[50]) electrode. The power spectrum in Figure 2 (b) shows roughness features in the size range of 10 nm to 10 μm. The morphological PSD is obtained using FE-SEM and the electrochemically obtained microscopic area. In order to capture the complexity arising from irregular SEM image, one often uses the fractal models.[51,52] The random fractal irregularities are usually understood in terms of their power law power spectrum. As shown in Figure 2 (a) and (b), most of the rough surfaces through their (intermediate wavelength) PSD can be approximately mapped into finite self-affine fractals (which exhibit scale invariance over a limited range of length scales).[48,49] The power law dependence of the power spectrum of finite-fractal over the limited scales of wavenumbers/wavelengths $(\vec{K}_{\parallel})$ is[20,53,54]

$$\left\langle |\hat{\zeta}(\vec{K}_{\parallel})|^2 \right\rangle = \ell_{\tau}^{2D_H-3}\, |\vec{K}_{\parallel}|^{2D_H-7} \quad \text{for} \quad 1/L \le |\vec{K}_{\parallel}| \le 1/\ell \tag{8}$$

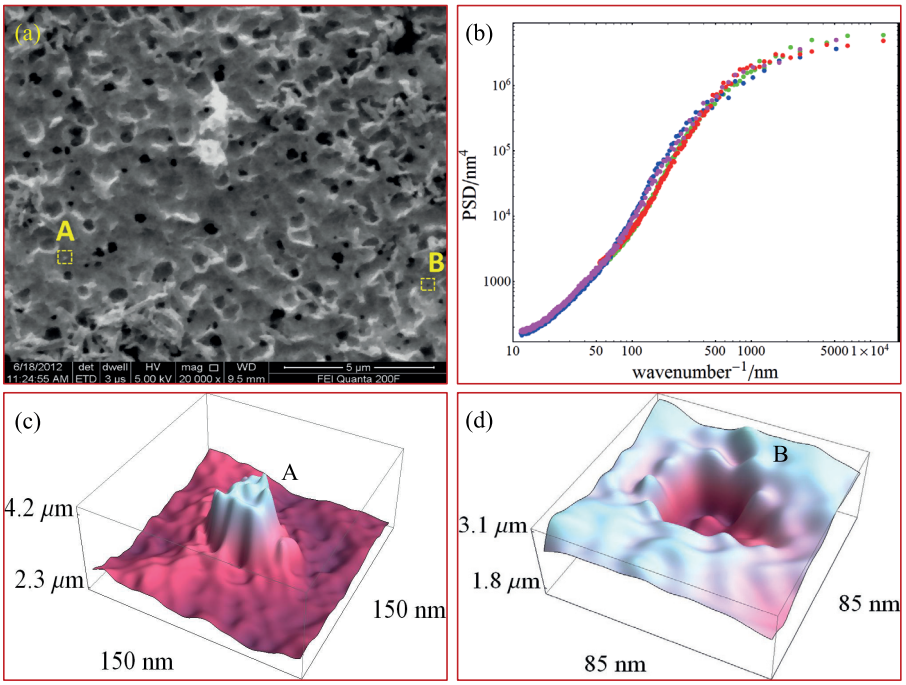

Figure 2: Quantitative reconstruction of electrode surface and its (a) FE-SEM micrograph and (b) power spectrum. Reconstruction of local surface profile at sites A and B showing (c) nanopimple and (d) nanopit.

where L is the sample size or upper cutoff length scale and D_H is the fractal dimension or Hausdorff-Besicovitch dimension. ℓ is the size of the finest feature of roughness and it denotes the length above which surface shows fractal behavior, i.e., roughness effects are seen. For ideal fractals, ℓ_τ is often the length at which the average slope on the surface will be equal to 1 radian, obtained by extrapolating power spectrum to wavenumber 1. However, it is established for real surfaces that the extrapolation method at wavenumber 1 often leads to unphysical results.[55] Typically, size range of ℓ_τ is 0.3–1.5 μm for mechanically and chemically roughened electrodes. Size of ℓ_τ determines the time upto which roughness effects will be observed in the current transient response. Wavenumbers between $1/\ell$ and $1/\ell_\tau$ will influence the electrochemical response arising due to processes involving diffusion.

SEM images appear to be three dimensional, but they are in fact two dimensional as the magnitude of elevation is not known. As mentioned earlier, the methodology shown in Figure 1 can also be used to determine the width of interface $(h = \sqrt{\text{MSW}})$ from morphological PSD of FE-SEM images to reconstruct 3D surface. This quantitative measurement is of importance for investigations of objects with 3D topographic features. This methodology can also be used for the detailed geometrical analysis. Local geometrical features like peaks and pits can be analyzed with this method. Figures 2(c) and 2(d) show the detailed 3D reconstructed surface of peak and pit at the rough platinum electrode (shown in FE-SEM image as site A and B, respectively in Figure 2(a)). These local geometrical features and statistical roughness in synergy with phenomenological length scales are important in understanding the anomalies in an electrochemical response. Therefore, length scales involved in various electrochemical phenomena will be discussed in the following section.

3 Electrochemical Phenomena and Length Scales

Local curvature and work function. The correlation between the structural aspects of the electrode and various phenomena at its surface is often recognized as the basic cause of anomalous electrochemical responses. In a broader sense, an electrochemical system comprises three zones constituting the electrode, electrode/electrolyte interface and the electrolyte solution. Metal electrode influences phenomena such as charge transfer kinetics, adsorption (of solvent and electroactive/inactive species) and formation of electric double layer, through its work function, which in turn is related to its electronic capacitance.[56,58] This leads to a region of electronic screening in metals that extends upto a few atom thickness and is known as the Thomas-Fermi electronic screening length (l_{TF}), defined as

$$l_{TF} = \sqrt{\frac{2 \epsilon_0 \epsilon_m E_f}{3 n_0 e^2}}, \tag{9}$$

where ϵ_m is the metal dielectric constant (4.5–7.2),[58] E_F is the Fermi energy (1.6–14.3 eV),[59] ϵ_0 is the permittivity of the free space, and e is the electronic charge. n_0 is the average number density, which can be determined from the Fermi energy and reduced mass of electron (m) as

$$n_0 = \frac{2E_f}{3} D_f, \tag{10}$$

where D_f $\left(= 8\sqrt{2}\pi m^{3/2} \sqrt{E_f}/h^3\right)$ is the density of states[59] and h is the Planck's constant. The electronic screening distance in metals is small (~0.1–0.2 nm) because of high n_0 (0.9×10^{22} – 24.6×10^{22}/cm^3).[58] Graphite, being a semimetal, behaves more like a metal with electronic screening length of ~0.27 nm.[60]

The Thomas-Fermi length is important in determining one of the electronic property of the metal surface, viz. work function.[58] It can be defined as the amount of energy required to take an electron from the metal surface to a region at infinity (out of the influence of image forces). Work function has been recently formulated for metals based on the Thomas-Fermi approximation[58] as the work against the electrostatic self-capacitive energy of the disc of radius l_{TF} (over the smooth metal surface) and is defined as,

$$\phi_E^0 = \frac{e^2}{2\pi \epsilon_0 \epsilon_m l_{TF}}. \tag{11}$$

Evidently, the work function is controlled by the sub-nanometer electronic screening length and dielectric of metals. Hence, they are the most relevant parameters in determining the electronic and electrochemical properties of the metals. It is clear from Equation 11 that the work function through the electronic screening length depends on the Fermi energy, density of states and dielectric constant. Since the electronic properties are known to depend on the structural aspects of the electrode surface, hence the theoretical knowledge of variation of work function with size and shape is required. The increase of electronic work function with reducing size of the spherical nanoparticles has been experimentally observed.[61,62]

Hausdroff Besicovitch dimension: The measure of the local size of a set of points defining a space. For smooth shape it is an integer corresponding to its topology, for complex fractal structures it can be a non-integer.

Thomas-Fermi approximation: An approximation to describe the total energy of a many body system as a function (functional) of electron density assuming that the electrons are distributed uniformly in each small volume element but the electron density can vary from one volume element to the other.

Spherical particle geometry being the simplest, is often considered to be an inceptive model for various nanoparticles. The work function of a spherical particle (ϕ_E^s) is shown to be inversely related to the particle size r as[58,63,64]

$$\phi_E^s = \phi_E^0 + \alpha \frac{e^2}{4\pi \epsilon_0 r}, \tag{12}$$

where α is an elusive parameter whose value is often stated to be 1/2[63,65] or 3/8[64,66] based on various theoretical predictions and experimental fitting gives it to be 0.3.[67] However, our theory[58] predicts explicit dependence on the dielectric of metal with $\alpha = 2/\epsilon_m$. Since the typical metal dielectric constants lie in the range of 4.2–7.2 (see supporting information of ref[58]), the parameter α is therefore estimated to vary in the range of ≈0.22–0.44. Surprisingly, the mean value of estimated range is same as the proposed experimentally fitted value.[67]

Idealized spherical geometry of nanoparticles is over simplification for most of the nanostructures. Usually, functional nanostructures have complex morphologies, e.g. cluster, star, fern, cube etc., and these can be characterized through the variation of curvature over the surface. The curvature of the surface can be well characterized in terms of local mean ($1/R = 1/R_1 + 1/R_2$) and Gaussian ($1/R_1R_2$) curvatures where R_1 and R_2 are the local principle radii of curvatures. The curvature effects has been incorporated to Equation 11 through multiple scattering expansion methods.[56,57] The resultant local curvature dependent work function of the nanostructured electrodes is[58]

$$\phi_E = \phi_E^0 \left(1 + \frac{l_{TF}}{R} + \frac{3l_{TF}^2}{2R^2} - \frac{l_{TF}^2}{2R_1R_2} \right). \tag{13}$$

This equation is applicable for realistic electrodes consisting of several fine nanoscale surface features. The dependence on the shape is maximum when one of the principal radius of curvature is small (< 1 nm) while the discernible effects will persist upto 50 nm. The beauty of Equation 13 is that it can be applied for an arbitrary surface profile exhibiting varying curvature, e.g. rough surfaces. Figure 3 shows simulated scaled work function $\left(\phi_E^* = \phi_E / \phi_E^0\right)$ on multiscale rough surface such as 2D Weierstrass-Mendelbrot function[68] with mean square height fluctuation of 0.7 nm and lower cut-off length as 1.14 nm. Even for this slightly rough surface the deviation of work function can go upto ±10% depending upon the local convexity. The charge transfer kinetics is exponentially related to the magnitude of work function,[69–71] therefore a small change in work function will cause large change in the kinetics.

From electrochemistry point of view, work function is closely related to the concepts of potential of zero charge (E_{pzc}), equilibrium or standard potential $\left(E_M^0\right)$[72] and the heterogeneous charge transfer.[69–71] For a metal electrode in contact with the solvent, the potential of zero charge is linearly related to the work function along with the corrections in the surface potentials caused due to metal solution contact.[73] So,

$$E_{pzc} = \frac{\phi_E}{e} + \delta\chi_M - g_{dipole}^S + K, \tag{14}$$

where $\delta\chi_M$ is the modification in the metal surface potential, g_{dipole}^S is the surface potential of solution in contact with the metal and K is a constant including the potential drop at the reference electrode/solution interface.[73] The absolute potential of a metal relative to a standard

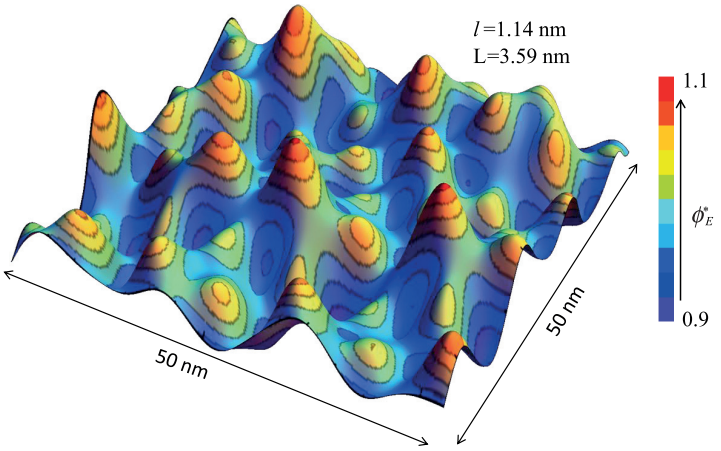

Figure 3: Simulated scaled work function on 2D Weierstrass-Mendelbrot finite fractal surface.

reference electrode gives the equilibrium or the standard electrode potential, E_M^0. Conventionally, the absolute potential is an intrinsic property dependent on the electrode work function, and is are related as[74]

$$e E_{abs}^M = \phi_E + e\Delta\psi_S^M, \tag{15}$$

such that $E_M^0 = E_{abs}^M - E_{abs}^{SHE}$ and $\Delta\psi_S^M$ denotes the contact potential difference between the metal and solution phase. Also, an important quantity usually used to characterize the catalytic or charge transfer activity is the exchange current density. Its relation to the electrode work function is given as[72]

$$\log i_0 = A\phi_E + B \tag{16}$$

where, A and B are the parameters obtained by fitting the experimental data.[72] Therefore, variation in the work function based on local surface curvature (from Equation 13) direct towards the active participation of electrode structure in influencing local electrochemical properties of thermodynamic nature. Consequently, work function emerges as an essential electrode characteristic, which strongly influences the electrochemical performance of a nanostructured metal electrode.[75]

Local curvature and electrochemical capacitance. Capacitance of an electrochemical system is dependent on various components, viz. the electrode type and structure, the electrode/electrolyte interfacial structure along with solvent dipoles and electrolyte concentration. An electrode in contact with a dipolar solvent has an interfacial region where the solvent dipoles exist in a specific orientation. This leads to variation in the interfacial surface potential resulting in capacity due to solvent dipole.[76] The dipole layer being analogous to the parallel plate capacitor can be considered to have thickness equal to the size of the dipole and charge density being the product of the dipolar charge and the number of oriented dipoles per unit area.[76] The maximum number of solvent molecules that can be packed over the electrode surface is again an intrinsic property of the shape and size of the electrode. While for a planar surface the parallel surface or the area of the locus surface of centroid of adsorbed solvent molecules has the same structure as that of the electrode, in case of curved electrode surfaces it gets modified. Relative to the planar surface this area is high over the convex and low over the concave features. So, the number density of the dipole molecules over these surfaces is modified accordingly. The nanostructuring induced variation in the surface dipole packing also influences the work function of the immersed metal electrode[77] through the variation in the surface potential of the metal electrode due to solvent contact. In the case of structurally anisotropic solvent molecules, e.g. room temperature ionic liquids (RTILs) or some organic solvents, the dipolar compact layer is further modified by their electrode potential dependent multistate orientations. In order to capture the resultant anomalies, the modified multistate model has been formulated.[78] It incorporates the ion shape asymmetry dependent molecular properties and related relaxation dynamics in the compact layer. This model with two or three ion orientation states in the compact layer for systems with shape asymmetric cations explains such anomalous dynamics.[79,80]

Under the influence of the interface established between the electrode and electrolyte certain extent of reorganization tend to prevail on metal as well as the solution side creating an electric double layer (EDL). The most distinctive features of the EDL at the electrode/electrolyte interface is its ability to store charges in a small region close to the electrode. The EDL evolves as the consequence of the intrinsic electric field manifested by the metal electrode leading to a field driven orientation of the solvent ions/molecules at the electrode surface. EDL was modeled for the first time like a conventional parallel plate capacitor by Helmholtz,[81] which was then followed by several modifications in the electric double layer. The double layer thus established, comprises the inner Helmholtz layer (IHP) with adsorbed dipolar molecules (primarily solvent if specific electrolyte adsorption is absent). The adjacent layer is the region comprising the solvated ions, forming the outer Helmholtz layer (OHP) whose thickness is denoted by r_H. At the immediate region of the electrode surface the capacitance density of the Helmholtz layer (c_H) is dependent on the thickness of OHP. Hence,[82]

$$c_H = \frac{\epsilon_0 \epsilon_H}{r_H} \tag{17}$$

Here ϵ_H is the dielectric constant of the Helmholtz layer that ranges between 2–6. The electrochemical capacitance is strongly dependent on the electrode morphology due to change in packing in compact and diffuse layer in confined spaces and work function.[83]

For an electrolyte solution having electrolyte ionic strength I, the ionic redistribution is

characterized through the ionic screening length, l_D which is given as

$$l_D = \sqrt{\frac{\epsilon\epsilon_0 k_B T}{2N_A e^2 I}}. \quad (18)$$

Here ϵ is the dielectric constant of electrolyte solution, k_B is the Boltzmann constant, T is the temperature in Kelvin and N_A is the Avogadro's number. In accordance with the classical electrolyte theory l_D decreases with the increase of electrolyte concentration. But recent studies show that l_D follows classical electrolyte theory upto certain concentration, and beyond that it again anomalously increases[84] due to association of ions. Ion-association is prominent particularly with ions of high charge. Also, the electrostatic screening length in concentrated electrolytes has been experimentally found to increase with the concentration,[85] e.g. l_D ~ 0.2–4 nm for aqueous NaCl solution. However, for RTIL/propylene system l_D ~ 0.6–11 nm, and can reach upto the range of l_D ~ 5–10 nm for pure RTIL.[85] Further, the potential dependence of the ionic screening leads to the potential dependent effective Gouy length which is given as,[87]

$$l_D^{\text{eff}} = l_D / \cosh\left(\frac{e\phi_2}{2k_B T}\right). \quad (19)$$

Electronic spillover: The finite electronic density up to certain distance, beyond the metal surface.

Here ϕ_2 denotes the potential with respect to potential of zero charge. The charge dependent electrostatic interactions between the ions is further characterized by the dielectric screening length, the Bjerrum length. It denotes the separation at which the electrostatic interaction energy between two ions is comparable in magnitude to the thermal energy, $k_B T$ and is given as,

$$l_B = \frac{e^2}{4\pi\epsilon\epsilon_0 k_B T} \quad (20)$$

This length denotes the maximum length upto which the dielectric screening would prevail. Alternatively, the ionic and dielectric screening lengths are related as,

$$l_D = \frac{1}{\sqrt{8\pi l_B N_A I}} \quad (21)$$

At room temperature, for water $l_B \approx 0.7$ nm.

Electronic capacitance of micropores and curved nano-electrodes. In real applied electrode materials the complexity arises due to the pore structure with interconnected three-dimensional connectivity of pores of nonuniform shape and size. During an electrochemical process, the phenomenological length scales and electrode structural scales work in a concerted fashion. Consequently, the overall capacitance has the contribution from the electronic properties of the electrode and the ionic properties of the solution, leading to the concepts of electronic and ionic capacitance. The electronic characteristics of the metal surface are incorporated in the electronic screening length. Thus for a planar surface, the electronic capacitance density is given as[86]

$$c_E^0 = \frac{\epsilon_M \epsilon_0}{l_{TF}} \quad (22)$$

However for an electrode surface with arbitrary structures, an analytical result, based on the Thomas-Fermi approximation,[56] has been formulated to understand the effect of shape and size of the material on the electronic screening and hence the charge storage. The electronic capacitance will have strong influence in the capacitance of super-capacitors with walls studded with sub-nanopores. This work unravels the shape-dependent localization and enhancement and reduction of capacitance in the conducting nanomaterials. The electronic capacitance of cylindrical sub-nanopores of radius r, with inclusion of the electronic spillover correction, is given as[56]

$$c_E = c_E^0\left(1 + \frac{l_{TF}}{2r_a} - \frac{l_{TF}^2}{8r_a^2}\right), \quad (23)$$

where r_a is the electronic spillover corrected radius of nanopore, viz. $r_a = r - l_{TF}/2$. Consequently, the electronic capacitance density for an arbitrary shaped metal electrode is obtained in terms of the ratio of the electronic screening length and the local radii of curvatures as[56]

$$c_E = c_E^0\left[1 - \frac{l_{TF}}{R} - \frac{l_{TF}^2}{2}\left(\frac{1}{R^2} - \frac{1}{R_1 R_2}\right)\right] \quad (24)$$

Since the electronic capacitance denotes the self consistent tendency of the metal electrode to store the electronic charge at its own surface, it is also known as the electronic self-capacitance.

Curvature and ionic capacitance. On the other hand, the ionic capacitance is dependent on the ionic structure of the electrolyte solution

and is also influenced by the morphology of the electrode. The ionic screening length (l_D) being a characteristic length denotes the region over which the significant charge separation persist. Hence, for the planar electrode surface the ionic capacitance density is given as

$$c_0 = \frac{\epsilon\epsilon_0}{l_D} \tag{25}$$

In order to incorporate the effect of electrode structure to the electrochemical capacitance, an equation for capacitance is obtained using a linear Gouy-Chapman or Debye-Huckel equation for the potential near the complex-geometry electrode-electrolyte interface.[87] Based on this theory, the ionic capacitance density for simple cylindrical nanopore is given as[87]

$$c_G = c_0\left(1-\frac{l_D}{2r_a}-\frac{l_D^2}{8r_a^2}\right). \tag{26}$$

The complex nature of the nanoporous electrode may also result in various distributions of surface shapes (curvatures) and pore lengths. This theory can effectively characterize the consequent deviations in the pore capacitance density through the fluctuations in the mean and Gaussian curvatures.[87] In general the capacitance density at the diffuse layer for arbitrary electrode structure is expressed in terms of the ratio of Gouy screening length (l_D) to the local principal radii of curvatures of the surface as[87]

$$c_G = c_0\left[1-\frac{l_D}{R}-\frac{l_D^2}{2}\left(\frac{1}{R^2}-\frac{1}{R_1R_2}\right)\right]. \tag{27}$$

For nano- and mesoporous electrode composed of porous Carbide Derived Carbon (CDC material), anomalous behavior in the capacitance has been observed by Gogotsi et al.[88–90] Their experimental results show three regimes in the capacitance vs pore size data (i) a nonlinear increase in capacitance, (ii) the transition from micropore to mesopore capacitance with a minimum, and (iii) the anomalous increase and a maximum in capacitance of pores with size below 1 nm. In order to get theoretical insights into these observations, Huang and co-workers[91–93] proposed a heuristic model for the capacitance with an assumption of cylindrical pores. Also, simulations of EDLs have been done that take into account the dependence of the electrolyte dielectric permittivity on the local electric fields[94] in spheres and with electrodes made of closely packed monodisperse mesoporous spheres.[95] However, these studies do not account for the detailed influence of the local shape, topology, and roughness on the electrochemical capacitance.

Several attempts have been made to explain the pore size dependence of the capacitance in micropores. Some of those perspectives include desolvation mechanism in an organic electrolyte,[96] electrostatic image energy contribution,[97,98] and atomistic molecular dynamics simulation for an ionic liquid confined inside a idealized nanotube.[60,99] However, some theories predict an oscillatory behavior in specific capacitance with the changing pore size.[100,101] Based on the modified Donnan model and with the assumption of a constant electrostatic potential inside a pore, an adsorption based theory has been presented by Kant and coworkers.[87] The theory accounted for the quantum mechanical contributions from electronic space charge (i.e., generalized Thomas-Fermi quasiclassical theory for electronic screening capacitance) and ion adsorption (i.e. adsorption capacitance) in the micropores.[87] Such that the capacitance of a micropore, c, is given as

$$c^{-1} = c_E^{-1} + c_{ad}^{-1}, \tag{28}$$

where, c_{ad} is the capacitance contribution due to the ion adsorption and is obtained by combining a modified Donnan model and an electric wire in cylinder capacitor (EWCC) model,[87] and is given as

$$c_{ad} = \frac{\epsilon\epsilon_0}{r_a \ln(r_a/a)}, \tag{29}$$

where r_a is the radius of the pore and a denotes the effective radius of the inner cylindrical wire due to an adsorbed ion and is dependent on the penetration length of the ion l_p and micropore density n_p, such that[87]

$$a = \sqrt{\frac{4a_0^3 n_0}{3n_p l_p}}\exp\left(\frac{-z_i e\Delta\phi_D + \mu_{att}}{2k_BT}\right). \tag{30}$$

Here, a_0 is the radius of bare ion, n_0 is the bulk ion density, $\Delta\phi_D$ is the Donnan potential and μ_{att} is the attraction term of ions adsorbing in micropores in the absence of applied potential.

4 Dynamic Response on Rough Electrodes and Length Scales

It has been already stated that the electrode surface has disorder and ex-situ microscopy

techniques offer high spatial resolution way to characterize the surface morphological disorders. Local morphology information obtained from FE-SEM, AFM etc. can be used in two ways to develop the theoretical prediction of electrochemical response of rough electrode, as shown in Figure 4. Local morphology information upon ensemble averaging gives the statistical morphological information of the rough surface. This information is further used in theoretical results at the disordered electrode to predict global electrochemical response over the electrode surface. Ensemble averaging en route is widely explored by Kant and coworkers, to theoretically predict global electrochemical response of the rough/disordered electrodes,[17–45] which will be discussed shortly. Local morphology information can also be used in another way around (refer Figure 4), i.e. to predict the local spatio-temporal electrochemical response of the disordered electrode, which upon surface averaging will give the global response. First, theoretical development is made in this direction. Local electrochemical impedance response is predicted for a reversible charge transfer system at 1D Weierstrass fractal electrode.[102]

Extensive theoretical developments have shown that the electrochemical response of a rough electrode is controlled by the power spectrum of roughness. A generic mathematical structure of these response equations is shown in Figure 5. Electrochemical response of a rough electrode can be considered as the sum of the response of macroscopic (smooth) electrode and contribution from the roughness arising through the convolution of phenomenological length scales dependent operator with the morphological length scales dependent power spectrum. This brings in coupling between phenomenological (such as double layer, ohmic, diffusion, quasireversibility, adsorption, bulk kinetics) and morphological (ℓ and ℓ_τ) length scales in prediction of response of the rough electrode. Phenomenon dependent operator contains the information about the length scales arising due to various process taking place at a working electrode. Various phenomenological length scales and their dependence on constitutive parameters will be discussed. Power spectrum

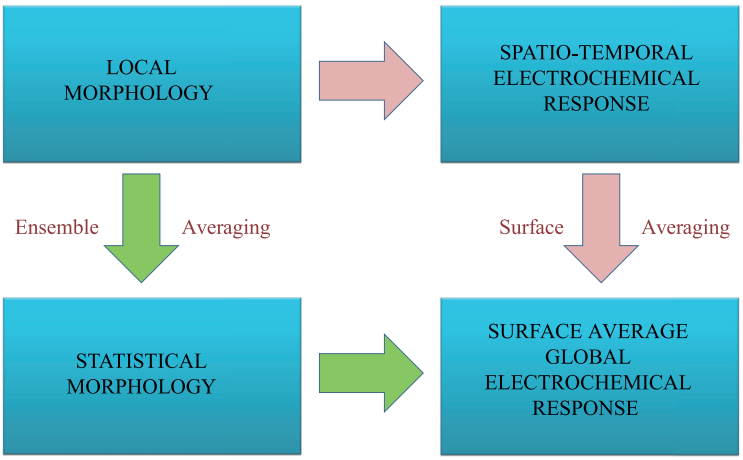

Figure 4: Theoretical dichotomy emerges due to two possible route to acquire global electrochemical response.

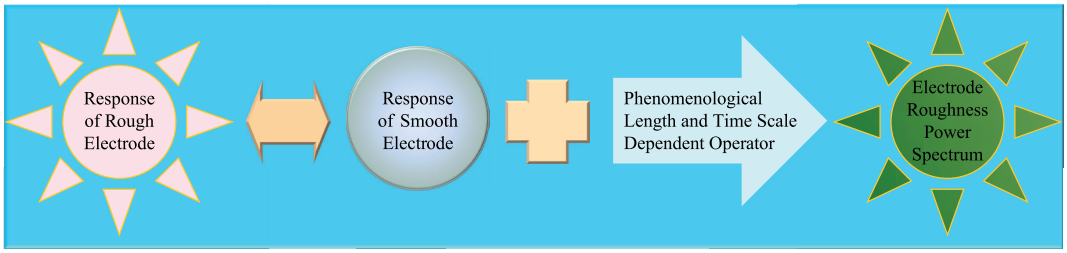

Figure 5: Structure of response equations for rough electrodes showing the controlling phenomenological length dependent operator and its convolution with PSD.

significantly controls the electrochemical response in the short and intermediate time regime. The long time regimes contribution from the power spectrum terms slowly decays and final response is controlled by the first term. Therefore, response of a rough electrode in the long time regime becomes identical to the smooth electrode response. Diffusion controlled system with fractal roughness shows anomalous intermediate time response, and the width of this regime also depends upon the viscosity of the electrolyte.[103]

The influence of roughness on the global electrochemical response through power spectrum based theories are extensively developed by Kant and his group for various electrochemical techniques. Roughness effects have been studied on the potential step chronoamperometric response in absence[17–23] or presence of uncompensated solution resistance.[24,25] Potential step chronoamperometry for diffusion controlled process has been extended to other electrochemical complexities such as partial diffusion-limited interfacial transfer/reaction with[26] or without uncompensated solution resistance[24,27] and bulk reaction coupling.[28] Double potential step chronoamperomtery (DPSC) is also studied using power spectrum based theory.[29] electrochemical impedance spectroscopy (EIS) is an also extensively studied technique using the power spectrum based theory for various processes such as admittance responses under the diffusion controlled processes,[30–32] diffusion with ohmic,[33] charge transfer coupled to bulk reaction (Gerischer admittance),[34] admittance response for the quasi-reversible system[35] and for adsorbed species.[36] Admittance response for Randles-Ershler model is also generalized.[37] Similarly, chronocoulometry technique for the diffusion limited case,[38,39] diffusion with uncompensated solution resistance[40] and coupled reactions[41] are reported. Voltammetry responses at a rough electrode for the diffusion limited process[42–45] are also predicted. These theories suggest that the power spectrum of randomly rough electrode is a natural characteristic that control its response. These theoretical models for realistic fractal geometry and methodology used for its characterization, has opened a new window to understand the influence of surface disorder. Experimental characterization[48,49,103,104] and their response validation[49,103,104] were performed recently, showing the influence of multi-scale roughness.

At phenomenological level the current transient at an electrode is manifested primarily by the diffusion process and the charge transfer kinetics. However, several parallel processes, viz. ohmic effects, random convection, specific ion adsorption tend to influence the overall electrode response. All these processes are further altered depending on the shape, size and roughness of the electrode and interface.

Diffusion: For a purely diffusion controlled process, the diffusion or depletion layer thickness has exponent equal to 1/2 in the time, frequency and scanning potential, see Table 1. However, the presence of multiscales or hierarchical nanofeatures can enhance (superdiffusion have effective exponent greater than 1/2) or slowdown (subdiffusion have effective exponent less than 1/2) the growth of diffusion layer thickness. This diffusion influenced anomalous response can be seen in the magnitude and phase (ϕ) of impedance spectroscopy.[30–32] The normal diffusion is identified with classical Warburg response having phase ϕ equal to 45°. For superdiffusion ϕ is greater than 45°, while for subdiffusion ϕ is less than 45°.[30–32] The anomalous Warburg impedance[31,33] on a finite fractal electrode roughness with ℓ ~10 nm to 100 nm shows superdiffusive behavior. The superdiffusive behavior is suppressed in the presence of quasireversibility,[24,26] uncompensated solution resistance,[25] coupling to bulk kinetics[27] and random convection[103] in the electrochemical system, and these processes also introduce subdiffusive behavior. In the case of charge transfer occurring via a diffusion controlled adsorption step, the superdiffusive behavior is further enhanced.[36] Depending on the viscosity of the reaction medium, the diffusion effects are typically seen from 10 nm to 10 μm in the absence of any other phenomena.

In electrochemical responses, roughness effects are observed over a period of measuring scale. Anomalous chronoamperometric behavior is seen between morphology dependent inner $\left(t_i \sim \ell^2/D\right)$ and outer $(t_o \sim \ell_\tau^2/D)$ crossover

Table 1: **Diffusion or depletion layer thickness for different electrochemical techniques.**

Chronoamperometry	$\delta(t)$	$\sqrt{\pi D t}$
Electrochemical impedance spectroscopy	$\delta(\omega)$	$\sqrt{D/\omega}$
Voltammetry	$\delta(e)$	$\sqrt{\pi D \frac{RT}{nFv}}$; $E \le E_p$ $\sqrt{\pi D \left\lvert\frac{E-E_p}{v}\right\rvert}$; $E > E_p$

D is the diffusion coefficient, t is the time, ω is frequency, R is the gas constant, T is temperature in Kelvin, n is the number of electrons transferred, F is the Faraday constant, E is the electrode potential, E_p is the peak electrode potential and v is the scan rate.

time scales.[21] At early time ($t < t_i$) when diffusion length is smaller than finest feature of surface, the electrode behaves as a smooth electrode with an enhanced area. While at long time ($t > t_o$) when diffusion length is larger than the width of roughness, chronoamperometric response is similar to the response at smooth electrode. Similarly, anomalous behavior is seen in response of impedance in between outer ($\omega_o \sim D/\ell^2$) and inner ($\omega_i \sim D/\ell_\tau^2$) cross over frequencies.[31,32] For the case of voltammetry, the effects of the electrode roughness can be recognized from the Cyclic Voltammograms (CV) by varying scan rates.[42] CV measurements in the low scan rate regime, that is, $\nu < \nu_\tau = 8\pi DRT/nF\ell_\tau^2$ are weakly influenced by the electrode roughness, and this regime behaves similar to the response of a smooth electrode for the diffusion limited case. Similarly, the measurements in high scan rate $\left(\nu > \nu_\ell = \pi DRT/nF\ell^2\right)$ are similar to the smooth electrode while the measurements in the intermediate scan rate $\left(\nu_\tau < \nu < \nu_\ell\right)$ is dynamically influenced by the roughness features.[42]

Ohmic effect on diffusion: Two types of ohmic losses are operative in the electrochemical systems, viz. 1) solution resistance of cell (R_s) and 2) uncompensated solution resistance (R_Ω) between Working (WE) and Reference (RE) electrodes responsible for the potential drop causing difference between applied and operative potentials.

R_s is the area specific resistance between Counter Electrode (CE) and working electrode (WE). R_s may depend on various ohmic contributions or the cell configuration. The characteristic size of diffusion length cut-off, due to presence of solution resistance of a cell, in a diffusion controlled system is[103]

$$l_c = \frac{nFC_O^0 D_O R_s}{2\Delta E}. \tag{31}$$

Here, R_s is the area specific solution resistance of the cell and $\Delta E = E - E^{0'}$. E is the potential step in chronoamperometry or the dc potential in impedance, or the initial potential step in voltammetry and $E^{0'}$ is the formal potential. For the case of rough electrode in presence of ohmic losses, detectable finest spatial resolution (l_c) will be usually greater than l, therefore the diffusion length will always be greater than $\delta(t)$, $\delta(\omega)$ or $\delta(E)$ (see Table 1). l_c is ~10 nm and ~100 nm in ionic liquid and aqueous medium, respectively.

R_Ω arises due to the separation between WE and RE. For any electrolyte medium, smaller the distance between WE and RE electrode, smaller is the value of R_Ω. Ohmic losses at the interfacial potential brings in pseudo-quasireversibility in the electron transfer kinetics and this apparent slowness in kinetics creates a diffusion-ohmic equilibration layer of thickness $\left(L_\Omega^\alpha\right)$;[24,25,103]

$$L_\Omega^\alpha = \frac{\sqrt{D_\alpha}\sqrt{D_O}}{k_\Omega} = \sqrt{D_\alpha}\left[\frac{n^2F^2}{RT}\frac{\xi\theta}{(1+\xi\theta)^2}\right]\left(\sqrt{D_O}C_O^0 + \sqrt{D_R}C_R^0\right)R_\Omega, \tag{32}$$

where k_Ω is the pseudo-kinetics (heterogeneous) rate constant and R_Ω is the uncompensated solution resistance. L_Ω^α is a function of concentration, diffusion coefficient D_α (α = O or R) and applied potential. Minimum value of L_Ω is ~30 nm and ~300 nm for RTIL and fully supported aqueous medium, respectively. Under large potential ($|\Delta E|$) step, L_Ω^α becomes negligible, as potential dependent factor ($\xi\theta/1+\xi\theta)^2$) in Equation 32 goes to 0. Similarly for sluggish kinetics where reaction current is small, diffusion-ohmic length becomes negligible. L_Ω^α shows symmetrical dependence around $E = E^{0'}$ and decreases on both sides of E.[103]

At the early time ($t < t_{i\Omega}$), transient response at a rough electrode is purely controlled by the uncompensated solution resistance. $t_{i\Omega} \sim L_\Omega^{\alpha 2}/D_\alpha$ is the inner crossover time or the ohmic-delay time upto which R_Ω effects will be seen on the response. Roughness induced anomalies in the transient response will be observed after $t_{i\Omega}$, and last upto the outer crossover time $\left(t_{o\Omega} \sim (L_\Omega^2 + \ell_\tau^2)/D\right)$. Beyond $t_{o\Omega}$, transient response of rough electrode is same as the response of a smooth electrode. In experimental data, the double layer charging current is found in short time regime of transient response in viscous or ionic liquid media. The characteristic electric double layer charging time (t_{dl}) is a measure upto which double layer charging inhibits (or delays) the faradaic processes, viz. $t_{dl} \approx R^* R_\Omega C_{dl}$. C_{dl} is the area specific capacitance. Hence, the delay in charge transfer processes induced by double layer charging increases with the increase in R_Ω, and will be large in viscous medium. Therefore, the effective delay time or inner crossover time in the experimentally measured transient response will be a combination of double layer charging (t_{dl}) and ohmic delay ($t_{i\Omega}$) time, viz. $t_{dl} + t_{i\Omega}$.

Quasireversibility: Rough electrodes with charge transfer equilibration layer thickness for facile kinetics (L_Q ~ 1 nm) with negligible ohmic (or IR) losses show dynamic diffusion controlled

regime for dense nanostructures, and (particle size ℓ dependent) steady state response for sparse nanostructures. Charge transfer equilibration layer thickness can be seen upto 10 μm for the sluggish kinetics. For unequal diffusion coefficients of oxidized and reduced species ($D_O \neq D_R$), charge transfer equilibration layer thickness or diffusion-kinetics length is defined as[24,27]

$$L_Q^{\alpha} = \frac{\sqrt{D_{\alpha}}\sqrt{D_O}}{k_f(1+\xi\theta)}, \tag{33}$$

where k_f is the surface-potential dependent forward rate constant,[24,27] $\theta = e^{-nf(\Delta E)}$ and $\xi = \sqrt{D_O/D_R}$. For equal diffusion coefficients, it is similar to the earlier reported results.[24,27] Effects of L_Q^{α} are predominantly seen in short time regime ($t < t_{iQ}$ where $t_{iQ} = L_Q^{\alpha 2}/D_{\alpha}$). L_Q^{α} defines an equilibration length near the interface having homogenized concentration profile. At short time, diffusion length $\left(\sqrt{\pi D_{\alpha} t}\right)$ is smaller than L_Q^{α}. Therefore, current transient in the short time regime is significantly kinetics and roughness controlled. Maximum effect of kinetics and roughness will be seen at the characteristic time $\sim \ell_{\tau} L_Q^{\alpha}/D_{\alpha}$. As time grows, diffusion length increases and suppresses the diffusion-kinetics length. In such cases, the process becomes diffusion controlled showing anomalous behavior due to electrode roughness upto outer crossover time $\left(t_{oQ} \sim (L_Q^{\alpha 2} + \ell_{\tau}^2)/D_{\alpha}\right)$. At long time regimes ($t > t_{oQ}$), rough electrode response behaves as a smooth electrode.

Quasi-reversibility in presence of ohmic contribution: Kinetics of quasireversibility and uncompensated solution resistance, the apparent diffusion-kinetics equilibration layer thickness is combination of kinetics and ohmic length, viz. $L_{Q\Omega} = L_Q + L_{\Omega}$;[26] thereby stating that the effective heterogeneous kinetics rate constant is the harmonic average of $k_{f/b}$ and k_{Ω}. Typical range of influence of L_{Ω} can be extended, for small potential steps, upto 100 μm, while for L_Q the range is 1 nm to 10 μm. But effects of L_Q are not observable and gets suppressed. Ohmic effects at the interfacial potentials lead to pseudo-quasireversibility in electron transfer kinetics that range from ~1 nm-10 μm. Presence of uncompensated solution resistance in a facile kinetics system leads to modification in the inner and outer crossover time scales as $t_{iQ\Omega} = L_{Q\Omega}^{\alpha\ 2}/D_{\alpha}$ and $t_{oQ\Omega} = (L_{Q\Omega}^{\alpha\ 2} + \ell_{\tau}^2)/D_{\alpha}$, respectively.[26]

Adsorption: The charge transfer process followed by the diffusion controlled adsorption relies on the extent of surface excess (Γ) of the electroactive species adsorbed at the surface. It has a characteristic penetration length, l_A, that denotes the extent of adsorption influence in the solution. It is defined as the ratio of change in surface excess to the change in concentration of adsorbing species at constant potential, and is given as,

$$l_A = \left(\frac{\partial \Gamma}{\partial C_{\alpha}}\right)_E, \tag{34}$$

Typical order of Γ for ions,[76] such as Cl^-, I^- and HSO_4^-, is 2×10^{-9} mol/cm^2, therefore l_A is ~20 nm and ~20 μm for concentrations of 1 M and 1 mM, respectively.

In a diffusion process, the adsorption influence is primarily concentrated at the electrode surface, leads to the surface adsorption capacitance (C_{ad}) that can be defined in the terms of l_A and the volume specific capacitance (Γ_W), such that $C_{ad} = \Gamma_W l_A$ where $\Gamma_W = n^2F^2/RT(1/C_O^0 + 1/C_R^0)$. Here n is the number of electrons transferred and C_O^0 and C_R^0 are the bulk concentrations of oxidized and reduced species, respectively. An interesting case of adsorption is the diffusion limited adsorption coupled to reversible charge transfer process on disordered electrode.[36] There are three characteristic crossover timescales observed in this case: (i) adsorption crossover time scale: $t_A \sim l_A^2/D$; for $t \geq t_A$ the system is adsorption controlled, (ii) intermediate time adsorption-diffusion coupling crossover regime: $t_A > t \sim t_q$ system follows adsorption-diffusion controlled, and roughness induced pseudo-quasireversibility time: $t_q \sim \ell_{\tau} l_A/D$ (iii) short time fractal crossover regime: $t_i \sim \ell^2/D$; $t_q > t > t_i$ shows anomalous response regime. These three characteristic times separate three processes, i.e. purely adsorption, mixed adsorption-diffusion-roughness and purely diffusion controlled regimes.

Cross over times: The characteristic time corresponding to the temporal transition of an electrochemical response.

Influence of random convection: As time ascends the system tends to acquire the steady state response. At long time or small frequency domain the random convection is manifested, thereby controlling the steady state response. At longer length scales, the phenomenon of random convection flow significantly influence the electrochemical response due to its dominance over the diffusive process. Depending upon the solution viscosity the magnitude of random flow velocity may vary from 50 nm/s to 0.5 μm/s. The random movement of fluids is described by hydrodynamics and is characterized by the hydrodynamic layer thickness, δ_H. For a solution having kinematic viscosity of ν and the random convection onset

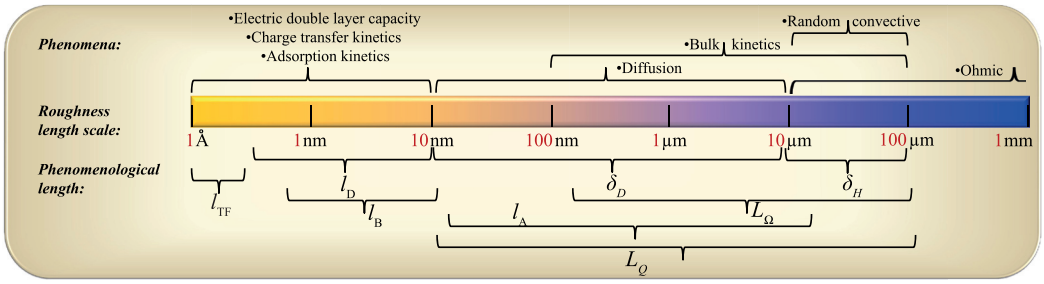

Figure 6: Synergistic effect of morphological and phenomenological length scales in disordered electrochemical system.

time as t_H (~40 ms), δ_H for αth electroactive species is defined as,[105]

$$\delta_H = \left(\frac{\nu}{D_\alpha}\right)^{1/3} \sqrt{\pi D_\alpha t_H} \qquad (35)$$

δ_H is of the order of 10–100 μm, and hence the random convection will influence the current transient in the intermediate and the long time regimes. Consequently, the convection contributions dominates over diffusion process over a long time, therefore diffusion control will persist only upto limited time scales.

Charge transfer coupled to bulk reaction: Another process which dominates at longer time scales is the presence of bulk kinetics (with k as the pseudo-first order rate constant) coupled to charge transfer at electrode, i.e. steady state current will be observed for time $t > 1/k$.[28] Similarly, constant impedance will be observed at lower frequency $\omega < k$.[34] This cross over to steady state behavior can be looked upon as the curtailment of diffusive behavior. The characteristic emergent time scale around which there will be maximum coupling between homogeneous kinetics and roughness is $\sim\sqrt{\ell_\tau^2/(kD)}$.

5 Summary and Future Perspective

In this review we have summarized the work done on the electrochemical properties and response under the influence of electrode sub-nanometer to micrometer scale of morphological disorders and roughness. Two generic theoretical approaches developed by Kant and coworkers, viz. (1) the curvature based theories suitable for processes with small phenomenological length scales and (2) the roughness power spectrum based theories are suitable for processes with intermediate and large phenomenological length scales, are addressed. Focus is kept on phenomenon and their length scales involved in controlling the electrochemical response on morphologically disordered electrodes. The knowledge of length scales addressed here can be used to further develop the scaling concepts in electrochemistry of disordered electrodes. All these morphological length scales and their interactions with the phenomenological length scales are shown in comprehensive manner in Figure 6. The figure shows various relevant phenomenological length scales of electrochemistry: (1) Thomas-Fermi electronic screening length (l_{TF}), (2) Debye ionic screening length (l_D), (3) adsorption solution penetration length (l_A), (4) Bjerrum dielectric screening length (l_B), (5) diffusion length (δ_D), (6) hydrodynamic layer thickness (δ_H), (7) ohmic-diffusion equilibration layer thickness (L_Ω) and (8) kinetics-diffusion equilibration length (L_Q). The extent of interaction of morphological length scales with these phenomena are listed above the scale.

Theories by Kant and coworkers allow the use of statistical information of morphology through microscopy to predict the global electrochemical response of disordered electrodes. Another futuristic approach is to understand and develop the theoretical frameworks for local electrochemical response through high spatial resolution microscopy of the electrode.

Acknowledgment

This work was supported by the grants from University of Delhi, India under "Scheme to Strengthen R&D Doctoral Research Programme", DST-SERB (Project No. SB/S1/PC-021/2013)-India and UGC India.

Received 9 September 2016.

References

1. E. Bakker and M. Telting-Diaz, Electrochemical sensors, *Anal. Chem.*, **74**, 2781–2800 (2002).
2. U. Yogeswaran and S. Chen, A review on the electrochemical sensors and biosensors composed of nanowires as sensing material, *Sensors*, **8**, 290–313 (2008).

3. D. Grieshaber, R. MacKenzie, J. Vörös and E. Reimhul, Electrochemical biosensors—Sensor principles and architectures, *Sensors*, **8**, 1400–1458 (2008).
4. D.R. Rolison and L.F. Nazar, Electrochemical energy storage to power the 21 st century, *MRS Bull*., **36**, 486–493 (2011).
5. D.W. Flaherty, N.T. Hahn, R.A. May, S.P. Berglund, Y.M. Lin, K.J. Stevenson, Z. Dohnalek, B.D. Kay and C.B. Mullins, Reactive ballistic deposition of nanostructured model materials for electrochemical energy conversion and storage, *Acc. Chem. Res*., **45**, 434–443 (2012).
6. D. Grier, E.B. Jacob, R. Clarke and L.M. Sander, Morphology and microstructure in electrochemical deposition of zinc, *Phys. Rev. Lett*., **56**, 1264–1267 (1986).
7. R. Kant, J. Kaur and M.B. Singh, Nanoelectrochemistry in India, SPR: Electrochemistry, *RSC*, **12**, 236–278 (2013).
8. R.W. Murray, Nanoelectrochemistry: Metal nanoparticles, nanoelectrodes, and nanopores, *Chem. Rev*., **108**, 2688–2720 (2008).
9. R.R. Nigmatullin, The realization of the generalized transfer equation in a medium with fractal geometry, *Phys. Stat. Sol*. (*B*), **133**, 425–430 (1986).
10. J.Y. Go and S.I. Pyun, A review of anomalous diffusion phenomena at fractal interface for diffusion-controlled and non-diffusion-controlled transfer processes, *J. Solid State Electrochem*., **11**, 323–334 (2007).
11. P.G. de Gennes, Excitation transfer in random media, *C. R. Acad. Sci. Paris*, **295**, 1061–1064 (1982).
12. T. Pajkossy, Electrochemistry at fractal surfaces, *J. Electroanal. Chem*., **300**, 1–11 (1991).
13. J.Y. Go and S.I. Pyun, Theoretical approach to cell-impedance-controlled lithium transport through $Li_{1-\delta}CoO_2$ film electrode with fractal surface: Numerical analysis of generalised diffusion equation, *Electrochim. Acta*, **50**, 3479–3487 (2005).
14. J.R. Macdoald, J. Schoonman and A.P. Lehnen, Applicability and power of complex nonlinear least squares for the analysis of impedance and admittance data, *J. Electroanal. Chem*., **131**, 77–95 (1982).
15. B.A. Boukamp, A nonlinear least squares fit procedure for analysis of immittance data of electrochemical systems, *Solid State Ionics*, **20**, 31–44 (1986).
16. J.R. Macdoald, Impedance spectroscopy: Old problems and new developments, *Electrochim. Acta*, **35**, 1483–1492 (1990).
17. R. Kant, Can current transients be affected by the morphology of the nonfractal electrode?, *Phys. Rev. Lett*., **70**, 4094–4097 (1993).
18. R. Kant, Can one electrochemically measure the statistical morphology of a rough electrode?, *J. Phys. Chem*., **98**, 1663–1667 (1994).
19. R. Kant and S.K. Rangarajan, Effect of surface roughness on diffusion-limited charge transfer, *J. Electroanal. Chem*., **368**, 1–21 (1994).
20. R. Kant, Diffusion-limited reaction rates on self-affine fractals, *J. Phys. Chem. B*, **101**, 3781–3787 (1997).
21. S.K. Jha, A. Sangal and R. Kant, Diffusion controlled potentiostatic current transients on realistic fractal electrodes, *J. Electroanal. Chem*., **615**, 180–190 (2008).
22. R. Kant and S.K. Jha, Theory of anomalous diffusive reaction rates on realistic self-affine fractals, *J. Phys. Chem. C*, **111**, 14040–14044 (2007).
23. R. Kant, General theory of arbitrary potential sweep methods on an arbitrary topography electrode and its application to random surface roughness, *J. Phys. Chem. C*, **114**, 10894–10900 (2010).
24. R. Kant and S.K. Rangarajan, Diffusion to rough interfaces: Finite charge transfer rates, *J. Electroanal. Chem*., **396**, 285–301 (1995).
25. S. Srivastav and R. Kant, Theory of generalized Cottrellian current at rough electrode with solution resistance effects, *J. Phys. Chem. C*, **114**, 10066–10076 (2010).
26. R. Kant, M. Sarathbabu and S. Srivastav, Effect of uncompensated solution resistance on quasireversible charge transfer at rough and finite fractal electrode, *Electrochim. Acta*, **95**, 237–245 (2013).
27. S.K. Jha and R. Kant, Theory of partial diffusion-limited interfacial transfer/reaction on realistic fractals, *J. Electroanal. Chem*., **641**, 78–82 (2010).
28. S.K. Jha and R. Kant, Theory of potentiostatic current transients for coupled catalytic reaction at random corrugated fractal electrode, *Electrochim. Acta*, **56**, 7266–7275 (2010).
29. S. Dhillon and R. Kant, Theory of double potential step chronoamperometry at rough electrodes: Reversible redox reaction and ohmic effects, *Electrochim. Acta*, **129**, 245–258 (2014).
30. R. Kant and S.K. Rangarajan, Effect of surface roughness on interfacial reaction-diffusion admittance, *J. Electroanal. Chem*., **552**, 141–151 (2003).
31. R. Kant, R. Kumar and V.K. Yadav, Theory of anomalous diffusion impedance on realistic fractal electrodes, *J. Phys. Chem. C*, **112**, 4019–4023 (2008).
32. R. Kumar and R. Kant, Generalized Warburg impedance on realistic self-affine fractals: Comparative study of statistically corrugated and isotropic roughness, *J. Chem. Sci*., **56**, 579–588 (2009).
33. S. Srivastav and R. Kant, Anomalous Warburg impedance: Influence of uncompensated solution resistance, *J. Phys. Chem. C*, **115**, 12232–12242 (2011).
34. R. Kumar and R. Kant, Theory of generalized Gerischer admittance of realistic fractal electrode, *J. Phys. Chem. C*, **113**, 19558–19567 (2009).
35. R. Kumar and R. Kant, Theory of quasi-reversible charge transfer admittance on finite self-affine fractal electrode, *Electrochim. Acta*, **56**, 7112–7123 (2011).
36. R. Kumar and R. Kant, Admittance of diffusion limited adsorption coupled to reversible charge transfer on rough and finite fractal electrodes, *Electrochim. Acta*, **95**, 275–287 (2013).

37. R. Kant and M.B. Singh, Generalization of Randles-Ershler admittance for arbitrary topography electrode: Application to random finite fractal roughness, *Electrochim. Acta*, **163**, 310–322 (2015).
38. R. Kant and Md. M. Islam, Theory of absorbance transients of an optically transparent rough electrode, *J. Phys. Chem. C*, **114**, 19357–19364 (2010).
39. Md. M. Islam and R. Kant, Generalization of the Anson equation for fractal and nonfractal rough electrodes, *Electrochim. Acta*, **56**, 4467–4474 (2011).
40. S. Srivastav and R. Kant, Influence of uncompensated solution resistance on diffusion limited chronocoulometric response at rough electrode, *Electrochim. Acta*, **180**, 208–217 (2015).
41. Md. M. Islam and R. Kant, Theory of single potential step absorbance transient at an optically transparent rough and finite fractal electrode: EC′ mechanism, *J. Electroanal. Chem.*, **713**, 82–90 (2014).
42. Parveen and R. Kant, Theory for anomalous response in cyclic staircase voltammetry: Electrode roughness and unequal diffusivities, *J. Phys. Chem. C*, **118**, 26599–26612 (2014).
43. Parveen and R. Kant, Theory for staircase voltammetry and linear scan voltammetry on fractal electrodes: Emergence of anomalous Randles-Sevcik behavior, *Electrochim. Acta*, **111**, 223–233 (2013).
44. Parveen and R. Kant, Theory for cyclic staircase voltammetry of two step charge transfer mechanism at rough electrodes, *J. Phys. Chem. C*, **120**, 4306–4321 (2016).
45. Parveen and R. Kant, General theory for pulse voltammetric techniques on rough and finite fractal electrodes for reversible redox system with unequal diffusivities, *Electrochim. Acta*, **194**, 283–291 (2016).
46. R.J. Adler, The geometry of random fields, Wiley, New York (1981).
47. A. Duparré, J. Ferre-Borrull, S. Gliech, G. Notni, J. Steinert and J. M. Bennett, Surface characterization techniques for determining the root-mean-square roughness and power spectral densities of optical components, *Appl. Optics*, **54**, 154–171 (2002).
48. S. Dhillon and R. Kant, Quantitative roughness characterization and 3D reconstruction of electrode surface using cyclic voltammetry and SEM image, *Appl. Surf. Sci.*, **282**, 105–114 (2013).
49. S. Srivastav, S. Dhillon, R. Kumar and R. Kant, Experimental validation of roughness power spectrum based theory of anomalous Cottrell response, *J. Phys. Chem. C*, **117**, 8594–8603 (2013).
50. A. Reiner, B. Steiger, G.G. Scherer and A. Wokaun, Influence of the morphology on the platinum electrode surface activity, *J. Power Sources*, **156**, 28–32 (2006).
51. B.B. Mandelbrot, The fractal geometry of nature, Freeman, San Francisco, CA (1977).
52. J. Feder, Fractals, Plenum press, New York (1988).
53. O.I. Yordanov and N.I. Nickolaev, Self-affinity of time series with finite domain power-law power spectrum, *Phys. Rev. E*, **49**, R2517-R2520 (1994).
54. R. Kant, Statistics of approximately self-affine fractals: Random corrugated surface and time series, *Phys. Rev. E*, **53**, 5749–5763 (1996).
55. L. De Chiffre, P. Lonardo, H. Trumpold, D.A. Lucca, G. Goch, C.A. Brown, J. Raja and H.N. Hansen, Quantitative characterisation of surface texture, *CIRP Ann.*, **499**, 635–642 (2000).
56. M.B. Singh and R. Kant, Shape and size dependent electronic capacitance in nanostructured materials, *Proc. Royal. Soc. A*, **69**, 20130163–20130174 (2013).
57. R. Kant, Electrochemistry at complex interfacial geometries, Thesis, Indian Institute of Science, Bangalore, (1993).
58. J. Kaur and R. Kant, Curvature-induced anomalous enhancement in the work function of nanostructures, *J. Phys. Chem. Lett.*, **6**, 2870–2874 (2015).
59. N.W. Ashcroft and N.D. Mermin, Solid state physics, Saunders college, Philadelphia (1976).
60. Y. Shim and H.J. Kim, Nanoporous carbon supercapacitors in an ionic liquid: A computer simulation study, *ACS Nano*, **4**, 2345–2355 (2010).
61. A. Schmidt-Ott, P. Schurtenberger and H.C. Siegmann, Enormous yield of photoelectrons from small particles. *Phys. Rev. Lett.*, **45**, 1284 (1980).
62. L. Zhou and M.R. Zachariah, Size resolved particle work function measurement of free nanoparticles: Aggregates vs. spheres, *Chem. Phys. Lett.*, **525–526**, 77–81 (2012).
63. D. M. Wood, Classical size dependence of the work function of small metallic spheres, *Phys. Rev. Lett.*, **46**, 749 (1981).
64. L.E. Brus, A simple model for the ionization potential, electron affinity, and aqueous redox potentials of small semiconductor crystallites, *J. Chem. Phys.*, **79**, 5566–5571 (1983).
65. J.M. Smith, Nonequilibrium ionization in wet alkali metal vapors, *AIAAJ*, **3**, 648–651 (1965).
66. L.E. Brus, Electron-electron and electron hole interactions in small semiconductor crystallites: The size dependence of the lowest excited electronic state, *J. Chem. Phys.*, **80**, 4403–4409 (1984).
67. M.D. Scanlon, P. Peljo, M.A. Méndez, E. Smirnov and H.H. Girault, Charging and discharging at the nanoscale: Fermi level equilibration of metallic nanoparticles, *Chem. Sci.*, **6**, 2705–2720 (2015).
68. N. Lin, H.P. Lee, S.P. Lim and K.S. Lee, Wave scattering from fractal surfaces, *J. Mod. Opt.*, **72**, 225–241 (1995).
69. S. Harinipriya and M.V. Sangaranarayanan, Electron transfer reactions at metal electrodes: Influence of work function on free energy of activation and exchange current density, *J. Chem. Phys.*, **115**, 6173–6178 (2001).
70. S. Harinipriya and M.V. Sangaranarayanan, Influence of the work function on electron transfer processes at metals:

Application to the hydrogen evolution reaction, *Langmuir*, **18**, 5572–5578 (2002).
71. J.O.M. Bockris and S.U.M. Khan, Surface electrochemistry, A molecular level approach, *Plenum press*, New York (1993).
72. S. Trasatti, Work function, electronegativity, and electrochemical behavior of metals, III: Electrolytic hydrogen evolution in acid solutions, *J. Electroanal. Chem.*, **39**, 163–184 (1972).
73. S. Trasatti, Work function, electronegativity, and electrochemical behavior of metals II: Potentials of zero charge and "electrochemical" work functions, *J. Electroanal. Chem.*, **33**, 351–378 (1971).
74. S. Trasatti, Structure of the metal/electrolyte solution interface: New data for theory, *Electrochim. Acta*, **36**, 1659–1667 (1991).
75. R. Kant and J. Kaur, Theory of shape and size dependent absolute/standard potentials of metal nanostructures, unpublished results (2016).
76. J.O.M. Bockris, A.K.N. Reddy and M.G. Aldeco, Modern electrochemistry fundamentals of electrodics (2A), second edition, Kluwer academic/plenum press, New York (2000).
77. J.M. Heras and L. Viscido, Work function changes upon water contamination of metal surfaces. *Appl. Surf. Sci.*, **4**, 238–241 (1980).
78. M.B. Singh and R. Kant, Theory of anomalous electric double layer dynamics in ionic liquids, *J. Phys. Chem. C*, **118**, 8766–8774 (2014).
79. M.B. Singh and R. Kant, Debye-Falkenhagen dynamics of electric double layer in presence of electrode heterogeneities, *J. Electronal. Chem.*, **704**, 197–207 (2013).
80. M.B. Singh and R. Kant, Theory of anomalous dynamics of electric double layer at heterogeneous and rough electrodes, *J. Phys. Chem. C*, **118**, 5122–5133 (2014).
81. H.F.L. Helmholtz, Studien über electrische grenzschichten, *Ann. Phys*. (Berlin), **243**, 337 (1879).
82. B.E. Conway, Electrochemical supercapacitor: Scientific fundamentals and technological applications Kluwer, Dordrecht (1999).
83. G. Gryglewicz, J. Machnikowski, E.L. Grabowska, G. Lota and E. Frackowiak, Effect of pore size distribution of coal-based activated carbons on double layer capacitance, *Electrochim. Acta*, **50**, 1197–1206 (2005).
84. R.A. Robinson and R.H. Stokes, Electrolyte solutions, Butterworths publications limited (1959).
85. A.M. Smith, A.A. Lee and S. Perkin, The electrostatic screening length in concentrated electrolytes increases with concentration, *J. Phys. Chem. Lett.*, **7**, 2157–2163 (2016).
86. O.K. Rice, Application of the Fermi statistics to the distribution of electrons under fields in metals and the theory of electrocapillarity, *Phys. Rev.*, **31**, 1051–1059 (1928).
87. R. Kant and M.B. Singh, Generalization of Gouy-Chapman-Stern model of electric double layer for a morphologically complex electrode: Deterministic and stochastic morphology, *Phys. Rev. E*, **88**, 052303 (2013).
88. P. Simon and Y. Gogostsi, Materials for electrochemical capacitors, *Nat. Mater.*, **7**, 845–854 (2008).
89. Y. Gogotsi, A. Nikitini, H. Ye, W. Zhou, J.E. Fischer, B. Yi, H.C. Foley and M. W. Barsoum, Nanoporous carbide-derived carbon with tunable pore size, *Nat. Mater.*, **2**, 591–594 (2003).
90. J. Chmiola, G. Yushin, Y. Gogotsi, C. Portet, P. Simon and P.L. Taberna, Anomalous increase in carbon capacitance at pore sizes less than 1 nanometer, *Science*, **313**, 1760–1763 (2006).
91. J. Huang, B.G. Sumpter, V. Meunier, G. Yushin, C. Portet and Y. Gogotsi, Curvature effects in carbon nanomaterials: Exohedral versus endohedral supercapacitors, *J. Mater. Res.*, **25**, 1525–1531 (2010).
92. J. Huang, B.G. Sumpter and V. Meunier, A universal model for nanoporous carbon supercapacitors applicable to diverse pore regimes, carbon materials, and electrolytes, *Chem. Eur. J*, **14**, 6614–6626 (2008).
93. G. Feng, R. Qiao, J. Huang, B.G. Sumpter and V. Meunier, Ion distribution in electrified micropores and its role in the anomalous enhancement of capacitance, *ACS Nano*, **4**, 2382–2390 (2010).
94. H. Wang and L. Pilon, Accurate simulations of electric double layer capacitance of ultramicroelectrodes, *J. Phys. Chem. C*, **115**, 16711–16719 (2011).
95. H. Wang, J. Vargehese and L. Pilon, Simulation of electric double layer capacitors with mesoporous electrodes: Effects of morphology and electrolyte permittivity, *Electrochim. Acta*, **56**, 6189–6197 (2011).
96. J. Chmiola, C. Largeot, P.L. Taberna, P. Simon and Y. Gogotsi, Desolvation of ions in subnanometer pores and its effect on capacitance and double-layer theory, *Angew. Chem. Int. Ed.*, **47**, 3392–3395 (2008).
97. S. Kondrat and A.A. Kornyshev, Superionic state in double-layer capacitors with nanoporous electrodes, *J. Phys. Condens. Matter*, **23**, 022201 (2011).
98. S. Kondrat, N. Georgi, M.V. Fedorov and A.A. Kornyshev, A superionic state in nano-porous double-layer capacitors: Insights from Monte Carlo simulations, *Phys. Chem. Chem. Phys.*, **13**, 11359–11366 (2011).
99. L. Yang, B.H. Fishbine, A. Migliori and L.R. Pratt, Molecular simulation of electric double-layer capacitors based on carbon nanotube forests, *J. Am. Chem. Soc.*, **131**, 12373–12376 (2009).
100. D. Jiang, Z. Jin, D. Henderson and J. Wu, Solvent effect on the pore-size dependence of an organic electrolyte supercapacitor, *J. Phys. Chem. Lett.*, **3**, 1727–1731 (2012).
101. G. Feng and P. T. Cummings, Supercapacitor capacitance exhibits oscillatory behavior as a function of nanopore size, *J. Phys. Chem. Lett.*, **2**, 2859–2864 (2011).
102. R. Kant, S. Dhillon and R. Kumar, Anomalous localization of electrochemical activity in reversible charge transfer at weierstrass fractal electrode: Local electrochemical impedance spectroscopy, *J. Phys. Chem. B*, **119**, 10876–10887 (2015).

103. R. Kumar, S. Dhillon and R. Kant, Influence of viscosity on chronoamperometry of reversible redox system on rough and nanoparticles deposited Pt electrode: Aqueous/glycerol and RTIL medium, *J. Electronal. Chem*., **780**, 337–354 (2016).
104. S. Dhillon and R. Kant, Experimental validation of the theory of chronoamperometry on nanoparticles deposited gold electrodes: Topography characterization through hybrid CV and SEM method, *Electroanalysis*, **26**, 2350–2357 (2014).
105. V.G. Levich, Physiochemical hydrodynamics, *Prentice-Hall Inc*., Englewood cliffs NJ (1962).

Rama Kant is currently working at University of Delhi. He obtained his Ph.D. degree from Indian Institute of Science, Bangalore in 1993 under the guidance of eminent theoretical electrochemist Prof. S.K. Rangarajan. His postdoctoral research experience includes working with Nobel laureate Professor P.G. de Gennes at college de France and Professor T.C.B. McLeish (FRS) at University of Leeds. Prof. Kant has made outstanding achievements in theoretical understandings of the electrochemical phenomena on rough/heterogeneous electrodes and complex nanostructured electrode. His significant contributions are the generalization of the fundamental equations of electrochemistry: Thomas-Fermi, Gouy-Chapman-Stern and Donnan for electric double layer capacitance of complex geometries, Cottrell, Anson, Danckwerts, Warburg and Gerischer for the reversible charge transfer at rough electrodes. He developed a novel method for quantitative roughness characterization and 3D reconstruction of electrode surface using cyclic voltammetry and FE-SEM images. Some other areas of his research interests include: Fractals, Dynamics of branched polymeric systems in solution and melts, and Dynamics of miscible polymer blends. He is the elected fellow of Indian Academy of Sciences and has been awarded the CRSI bronze medal.

Shweta Dhillon is a Ph.D. student under the guidance of Professor Rama Kant at University of Delhi. She did her M.Sc. with physical chemistry specialization in 2010 from University of Delhi. She has recently submitted her thesis entitled-Spatially Resolved Electrochemical Impedance Spectroscopy and Chronoamperometry on Disordered Electrodes: Theory, Experiment and CV - SEM Method. In Prof. Kant's group she has authored 5 publications in high impact peer-reviewed journals. Her current research interest is the study of local electrochemical behavior of rough electrodes using theoretical approach.

Jasmin Kaur is a Ph.D. student under the guidance of Professor Rama Kant at University of Delhi. She is working as a Senior Research Fellow in the Complex systems group of Prof. Kant. She graduated with a B.Sc.(H) degree in 2010 and M.Sc. degree in 2012 from University of Delhi. Her research interest is the study of the curvature dependent electronic properties of the metal nanostructures and their correlation with the electrochemical properties. By far in Prof. Kant's group, she has coauthored a review article in Specialist Periodical Report of Royal Society of Chemistry and is working on various projects in the field of Nanoelectrochemistry.